Random Flow Generation for Large Eddy Simulation
A Case Study on Building Aerodynamics

建築物空力解析における LES のための流入変動風生成手法の適用事例

LONG DOAN SY[*1], CHISATO KOJIMA[*1], MANABU KAWASHIMA[*1]
ドアン　セイ　ロン，小島　千里，川島　学

This study presents an overview of the Consistent Discrete Random Flow Generation (CDRFG) method, an efficient approach for generating synthetic inflow boundary conditions in Large Eddy Simulation frameworks. The method is implemented in a high-resolution computational fluid dynamics simulation comprising approximately 33.8 million mesh elements. The CDRFG technique successfully reproduces key characteristics of the vertical wind profile. Additionally, when applied to a high-rise building model, the front face pressure and along-wind force spectra in the wind direction are accurately reproduced. However, issues are identified in the reproducibility of wind pressure on side faces, and further efforts are needed to improve the accuracy of wind force predictions in the across-wind direction.

Keywords: CFD, LES, Random flow generation (RFG), Turbulence flow, High-rise buildings, Wind pressure coefficient, Wind tunnel experiment

本報では，LES による数値流体解析において流入境界条件を数値的に生成する手法である Consistent Discrete Random Flow Generation（Consistent Discrete RFG；CDRFG）法の概要と，3,380 万メッシュ規模の数値計算への適用事例を示す。CDRFG 法により，流入変動風の風速プロファイルの基本的な特性を良好に再現できた。高層建物モデルへの適用では，風向に正対する前面の風圧係数と風方向の風力スペクトルについて，既往の風洞実験結果を精度よく再現可能であった。一方，主に側面の風圧係数の再現性に課題が認められ，風直交方向の風力予測の精度向上に今後取り組む必要がある。

キーワード：CFD，LES，Random Flow Generation(RFG)，流入変動風，高層建築物，風圧係数，風洞実験

1. Introduction

In the field of wind engineering, the potential for evaluating wind loads using Large Eddy Simulation (LES) has been progressively established through guidelines issued by the Architectural Institute of Japan[1)] and related publications[2)]. However, the authors recognize two key challenges that hinder its practical application. The first involves ensuring that the computational resources and time required remain within a reasonable range, even if the calculations are theoretically feasible. The second challenge is to ensure the reliability of simulation results in a field that remains under active research and development.

To address these challenges, the authors have undertaken efforts aimed at the practical implementation of LES in wind-resistant design. In a previous study[3)], the authors examined the inevitable energy dissipation at the grid scale in

*1　Research & Development Institute, Technology Development Promotion Department

LES by referencing Kolmogorov′s energy spectrum, and discussed the relationship between the maximum wavenumber required for engineering purposes and mesh size.

This study presents a methodology to generating turbulent inflow conditions, which has received relatively little attention within the Japanese literatures, and demonstrates its application through the selected case study. The proposed approach, based on in prior research[4] conducted internationally, enables the imposition of the divergence-free condition on the velocity field by formulating the problem in the wavenumber domain. The fundamental principles underlying the employed waveform synthesis method are first outlined, followed by a detailed description of the analytical model. Subsequently, the paper presents representative results obtained from LES analysis utilizing this methodology.

2. Review of the Random Flow Generation method

The generation of synthetic turbulent inflow using waveform synthesis methods can be broadly classified into two main trends of research. The first trend originates from the method proposed by Hoshiya[5] and later developed by Kondo *et al.*[6], and recently Noda *et al.*[7), 8]. This approach is based on waveform synthesis in the frequency domain and enables the incorporation of the spatial structure of turbulence through power and cross-spectral density functions. Due to its computational efficiency, this method is considered practical for engineering applications. However, special attention must be paid to the enforcement of the divergence-free condition. For example, the method proposed by Kondo *et al.*[6] requires spectral corrections that allow for slight distortions in the power and cross-spectra to approximately satisfy this condition.

The second trend of research is originally introduced by Kraichnan[9] for generating isotropic turbulence, which was later formalized as the Random Flow Generation (RFG) technique by Smirnov *et al.*[10], and has been implemented in the boundary condition module of the commercial CFD software Ansys Fluent since version 12. Subsequently, Huang *et al.*[11] extended the theoretical framework to accommodate arbitrary energy spectra. Building on this, Aboshosha *et al.*[4] proposed a method for generating inflow turbulence that conforms to a von Karman-type power spectrum while approximately preserving spatial coherence. The present study adopts this approach of Aboshosha *et al.*[4] (referred to as the Consistent Discrete RFG, or CDRFG) due to its proven capability to reproduce realistic turbulent structures. Among existing inflow generation techniques, CDRFG is considered one of the most robust in capturing the spatial characteristics of turbulence. The fundamental principles of this method are outlined in the following.

The turbulent velocity components $u_i(x_j,t)$ at an arbitrary spatial location x_j for $i = x,y,z$ can be expressed using discrete wavenumbers $k_j^{m,n}$ and frequencies $f_{m,n}$ as follows:

$$u_i(x_j,t) = \sum_{m=1}^{M}\sum_{n=1}^{N}\left(p_i^{m,n}\cos\alpha_j^{m,n} + q_i^{m,n}\sin\alpha_j^{m,n}\right) \tag{1}$$

where $\alpha_j^{m,n} = k_j^{m,n}x_j^m + 2\pi f_{n,m}t$. This formulation incorporates both frequency and wavenumber components within the trigonometric basis functions. The spatial coordinate is normalized as $x_j^m = x_j/L_j^m$, where L_j^m is the characteristic length scale to be defined later. Once the weighting coefficients $p_i^{m,n}$ and $q_i^{m,n}$ are specified, the turbulent velocity field is fully defined. Thus, the development of methods to determine these coefficients has been a central focus in this trend line of research.

The indices n and m denote the segmentation of the turbulence waveform u_i: the n-th component out of N segments and the m-th realization out of M samples generated using normally distributed random numbers around each segment. Equation (1) therefore expresses u_i as a discretized sum in both wavenumber and frequency space.

Aboshosha*, et al.*[4], expanding upon the random number generation method introduced by Huang *et al.*[11], proposed a formulation for determining the weighting coefficients $p_i^{m,n}$ and $q_i^{m,n}$ using the following expressions, which satisfy the anisotropic spectral characteristics $S_{u_i}^m$:

$$p_i^{m,n} = \mathrm{sign}(r_i^{m,n}) \sqrt{\frac{1}{N} S_{u_i}^m \Delta f \frac{(r_i^{m,n})^2}{1 + (r_i^{m,n})^2}} \tag{2}$$

$$q_i^{m,n} = \mathrm{sign}(r_i^{m,n}) \sqrt{\frac{1}{N} S_{u_i}^m \Delta f \frac{1}{1 + (r_i^{m,n})^2}} \tag{3}$$

where Δf denotes the frequency interval between adjacent segments. The characteristic length scale is defined as $L_j^m = U/\gamma C f_m$, where U is the mean wind speed, f_m is the segment frequency, and γ, C are parameters as proposed in Aboshosha *et al.*[4]. This characteristic length is directly related to the spatial coherence properties of the generated turbulence field.

The divergence-free condition, which stems from the incompressibility constraint in the governing Navier‑Stokes equations, must be satisfied by the synthesized velocity field expressed in the form of equation (1). Taking the spatial divergence $\nabla \cdot u = 0$ leads to the following condition:

$$\begin{bmatrix} p_x^{m,n} & p_y^{m,n} & p_z^{m,n} \\ q_x^{m,n} & q_y^{m,n} & q_z^{m,n} \\ k_x^{m,n} & k_y^{m,n} & k_z^{m,n} \end{bmatrix} \begin{Bmatrix} k_x^{m,n} \\ k_y^{m,n} \\ k_z^{m,n} \end{Bmatrix} = \begin{Bmatrix} 0 \\ 0 \\ 1 \end{Bmatrix} \tag{4}$$

The unit norm of the wavenumber vector is a constraint that arises from the normalization of spatial coordinates using the characteristic length scale L_j^m. By employing an appropriate solver, one can determine the wavenumber vector $k_j^{m,n}$ corresponding to the weighting coefficients $p_i^{m,n}$ and $q_i^{m,n}$. Based on equation (4), waveform synthesis using the RFG-based approach inherently satisfies the divergence-free condition.

By substituting the obtained parameters into the summation in equation (1), the waveform synthesis can be executed, thereby enabling the generation of synthetic turbulent inflow. The computational cost associated with this process depends on the chosen values of M and N, which should be determined by balancing the trade-off between the desired spatial resolution and the available computational resources.

3. Verification of generation flow

3.1 Wind tunnel test data

This study utilizes publicly available[12] wind tunnel (WT) experiment data from Tokyo Polytechnic University, using a building model with width B = 100mm, depth D = 100mm and height H = 400mm, corresponding to a 1/400 scale of the prototype building. The flow profile corresponds to a power-law exponent α = 0.25. Time-resolved pressure data were recorded at 1,000Hz from 400 pressure taps across the building's side faces, with a total duration of 50 seconds.

3.2 Comparison of generation wind profile and WT data

CDRFG method is employed to synthesize the inflow turbulence. The available wind profile in WT experiment data provided the mean wind velocity profile and the turbulence intensity in the along-wind direction. Therefore, the turbulence intensity in the across-wind direction is assumed based on in-house previous WT experiment data corresponding to the same surface roughness conditions, characterized by a power-law exponent of α=0.25. The integral length scales in the across-wind is estimated using the empirical relation proposed by Counihan[13], where L_v = $0.33L_u$. The number of frequency segment M is set to 250, and the number of random frequencies in one segment N is set to 200. Vertical wind fluctuations are neglected in the present simulation.

Fig. 1 presents main characteristics of the inflow turbulence generation using the CDRFG method, illustrating key flow characteristics such as mean wind speed, turbulence intensity and power spectra density. **Fig. 1**(a) and **Fig. 1**(b) demonstrate that the method could reproduces essential atmospheric boundary layer properties, including the mean wind speed profile and turbulence intensity distribution when producing the flow properties is in good agreement with WT experimental data. **Fig. 1**(c) illustrates the power spectral density at the reference height H = 400mm, showing that the spectrum generated by the CDRFG method closely matches the theoretical Von Karman spectrum over a wide

frequency range. This agreement indicates that the method could capture the energy distribution across turbulent scales and preserves the characteristics of the inertial subrange. Considering the fundamental flow parameters, the CDRFG method could reproduce the inflow characteristics.

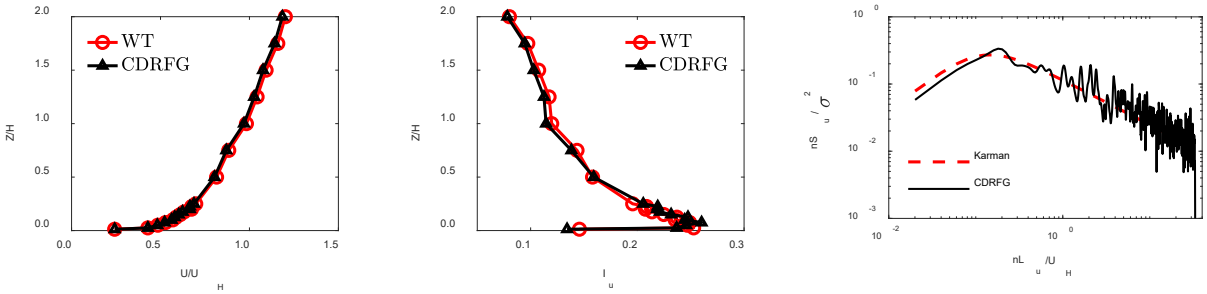

(a) Mean wind speed profile　(b) Turbulence intensity profile　(c) Power spectra density at height H

Fig. 1. Generation flow properties

4. Application of CDRFG in LES simulation of high-rise building model

4.1 Analysis model

The computational domain is illustrated in **Fig. 2**, and the simulation conditions are summarized in **Table 1**. The domain dimensions are set to 31B in the streamwise direction (x), 21B in the across-wind direction (y), and 18B in the vertical direction (z), where B = 100mm is the width of the building model. An unstructured grid system (tetrahedral) is employed and divided into seven zones corresponding to maximum mesh size indicated in the same figure. The configuration of the computational domain is originally based on the guideline from Architectural Institute of Japan[2], with a modification applied to zone ④ where the refined mesh region extends beyond the building vicinity to the inlet boundary, generating about 33.8 million mesh cell.

The inflow boundary generation points located at the inlet boundary (**Fig. 2**) and generated using the CDRFG method are uniformly distributed in both horizontal and vertical directions at the inflow plane. The spacing between adjacent points is set to 15mm, corresponding to approximately twice the minimum grid resolution of 8mm near the inflow boundary.

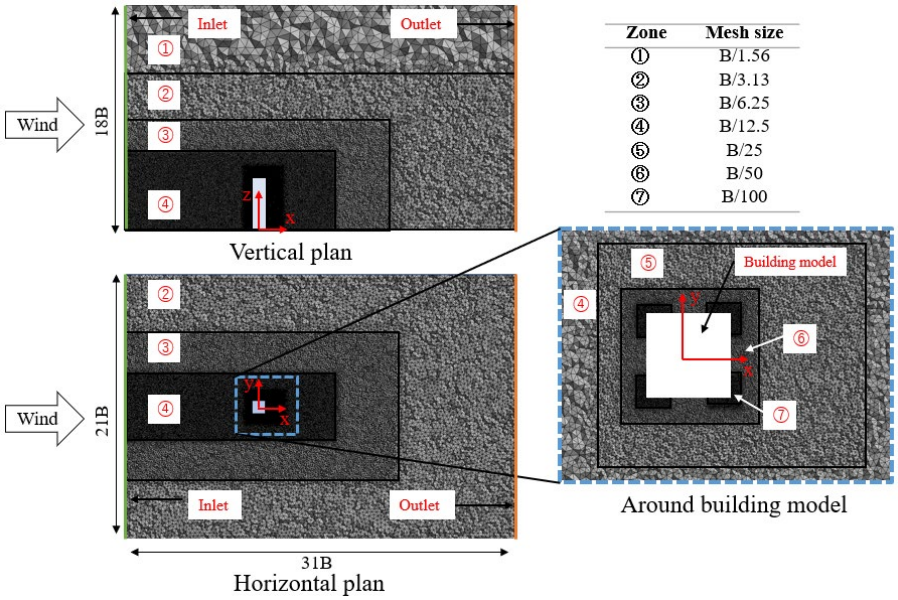

Fig. 2. Domain and mesh size

Table 1. Conditions for LES calculations

Software	OpenFOAMv2106
Subgrid-Scale model	Smagorinsky model Cs = 0.14
Time scheme	2nd order implicit
Convection scheme	2nd order Upwind
Diffusion scheme	2nd order Central
Boundary condition:	Inlet: CDRFG Wall, ground: Spalding wall function Top, side: Symmetry
Time step Δt	0.0001s
Sampling data	65536
Number of samplings	1

4.2 Results of the flow in domain without building model

Fig. 3 shows the vertical profile of mean wind speed, turbulence intensity, and power spectral density without the building model. The vertical axis is normalized by the height of building model, H. The profiles are centered in the y direction ($y = 0$) and x plans are positioned as shown in **Fig. 4**. The WT experiment data corresponds to the WT experiment results, taken at the center of the turntable. While the mean wind speed remains uniform across the streamwise direction, the turbulence intensity decreases notably from near inlet to $x = -5B$, and then decreases more slowly after that.

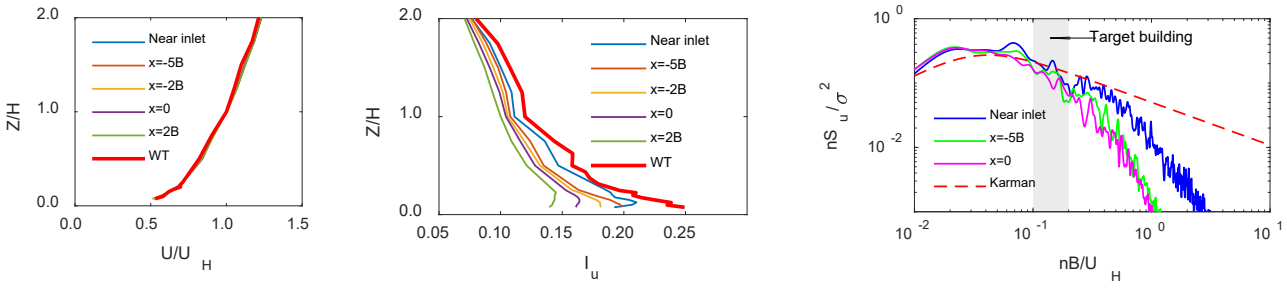

(a) Mean wind speed profile　(b) Turbulence intensity profile　(c) Power spectra at the model height

Fig. 3. Vertical wind profiles without building model

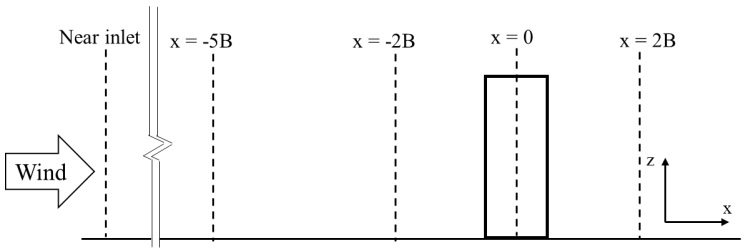

Fig. 4. X-coordinate positions for plotting wind profile

The power spectra in **Fig. 3**(c) generally matches the theoretical von Karman spectrum in low frequency range. However, as the flow progresses into the calculation domain, the high frequency components gradually attenuate. While this trend may partially reflect the natural decay of turbulence with downstream distance, it may also be influenced by the intrinsic filtering characteristics of the LES approach, which eliminates subgrid-scale motions above the cutoff frequency corresponding to the smallest turbulent scales resolvable by the mesh. In other words, this filtering is thought to have artificially reduced the spectral energy in the high-frequency band because the grid resolution in mesh zone ④, covering most of the area from the inflow point to the building location, may be limited in its ability to fully resolve grid-scale motions below the cutoff frequency, resulting in the inability to capture small-scale eddies. The shaded area labeled “Target building” in the figure indicates the frequency range estimated to contribute to the dynamic response of the building model. Notably, a slight attenuation of the power is also observed within this range.

4.3 Evaluate the wind load on building model

Fig. 5 presents comparisons of mean and peak pressure coefficients on each building face obtained from WT experiment (horizontal axis) and CFD (vertical axis). For the WT experiment data, five samples of 8 seconds (corresponding to 10 minutes in full-scale time) were extracted for analysis. Each plot point corresponds to the location where wind pressure is measured in the WT experiment. The peak pressure coefficients are calculated using a moving average of 0.5 seconds in real time. The dashed lines indicate a ±20% range based on WT experiment data. **Fig. 6** presents contour plots of the mean and peak wind pressure coefficients across the surfaces, offering a spatial representation of the data shown in **Fig. 5**. The subsequent discussion refers to the results illustrated in **Fig. 6**. On the front face, where positive pressure dominates, CFD results show good agreement with WT experiment results in both mean and peak values. This is likely due to the presence of large-scale, low-frequency flow structures in the frontal region, which are well preserved from the inlet to the building position in CFD. This finding is further supported by the contour plots shown in **Fig. 6**.

In regions where negative pressure dominates, the mean wind pressure coefficients generally show an agreement between CFD and WT experiment results. Despite this overall consistency, the sidewall results tend to exhibit slightly different values between CFD and WT experiment data, and this trend becomes relatively larger at the upper part of the building model. In more detail, the wind pressure coefficients on the sides in **Fig. 6** shows that CFD gives smaller mean amplitudes near the leading edge, while WT experiment data indicates large negative pressures near the leading edge that gradually weaken downstream. These results align with the trends reported by Yu *et al.*[14] and Chen *et al.*[15]. The contrasting trends at the side faces between CFD and WT experiment results suggest that the current CFD model may not adequately capture the development of shear layers and vortex interactions near the leading edge of the side surface. As shown in **Fig. 6**, on the rear face, the mean pressure distributions are generally consistent between CFD and WT experiment results, while peak values from CFD tend to be overestimated, especially in the regions of high negative pressure near the edges.

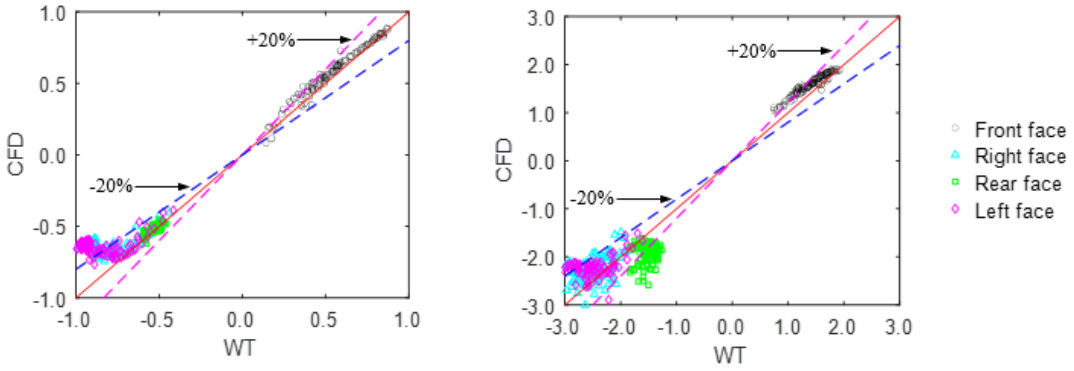

(a) Mean pressure coefficients　　(b) Peak pressure coefficients

Fig. 5. Comparison between CFD analysis and WT experiment

Fig. 7 shows the power spectrum density of forces and moments, including the along-wind force (C_{Fx}), across-wind force (C_{Fy}), overturning moment (C_{Mx}, C_{My}), and torsional moment (C_{Mz}). The red dashed line (AIJ Equa) represents the calculation results based on the Architectural Institute of Japan (AIJ) recommendations for Loads on Buildings[1]. Overall, CFD results demonstrate agreement with both WT experiment results and values derived from the recommendations of AIJ. In particular, the along-wind components (C_{Fx}, C_{My}) in CFD show good consistency with the WT experiment results, reflecting the accurate reproduction of the pressure distribution on the front face, which predominantly governs along-wind loads. Conversely, for the across-wind and torsional components, small discrepancies are observed between CFD and WT experiment results. These include a shift of peak frequencies toward lower ranges and a reduction in spectral power at higher frequencies. These discrepancies are considered to be

influenced by the limited reproducibility of the pressure distribution along the side surfaces, as well as a slight attenuation of wind speed power within the frequency range relevant to across-wind vibrations of the building model around the upstream domain. Nevertheless, the CFD analysis successfully predicts the peak overturning moment in the across-wind direction (C_{Mx}) in alignment with the AIJ load recommendation values. While the discrepancies between CFD and WT experiment results in across-wind direction is not examined further in the current paper, this matter remains a subject for ongoing investigation.

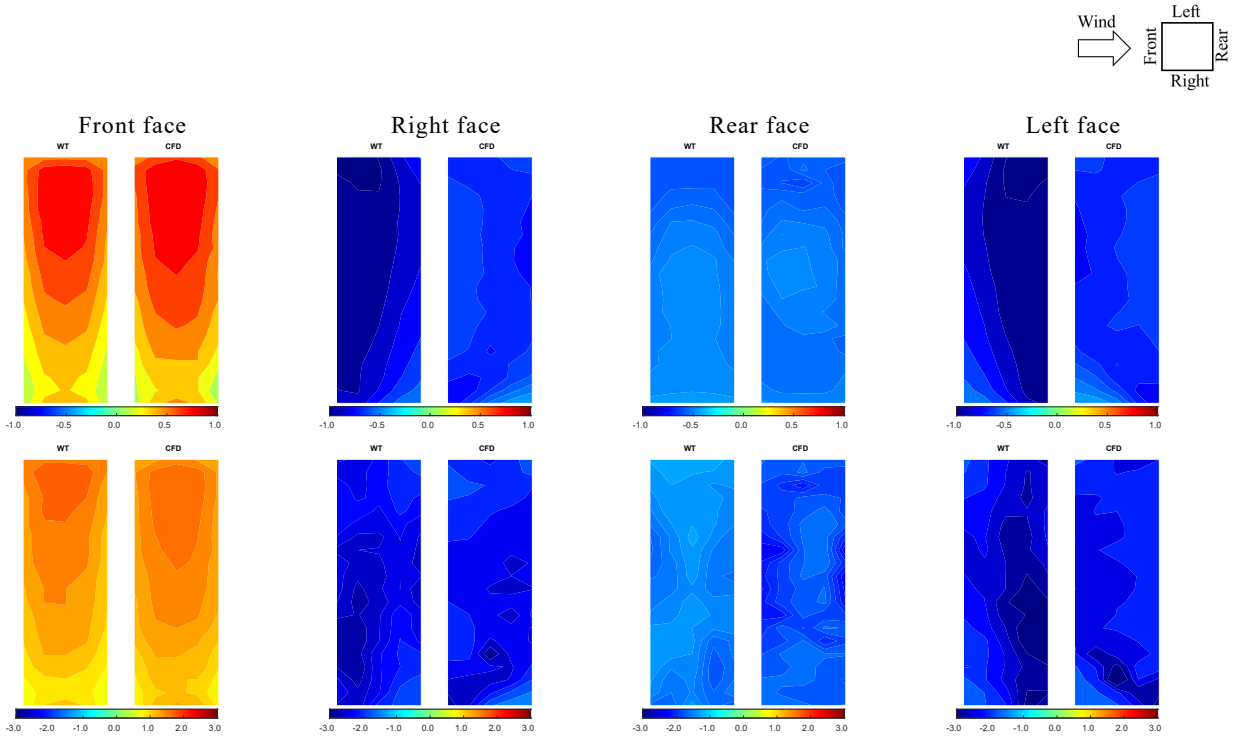

Fig. 6. Comparison of pressure contour on model's face between CFD analysis and WT experiment
Top row: Mean pressure coefficient; Bottom row: Peak pressure coefficient

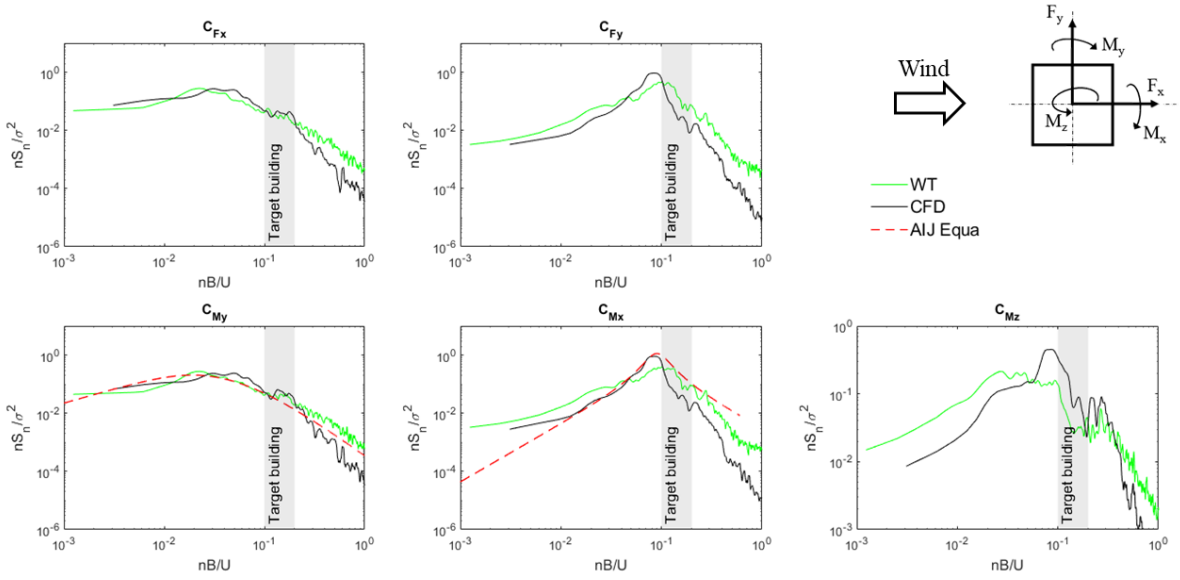

Fig. 7. Comparison of power spectra density of wind force coefficients between CFD and WT experiment

5. Conclusions

This study introduced the CDRFG method, which incorporates wave number information, as an effective approach for generating synthetic inflow turbulence in LES. The method successfully reproduced key boundary layer characteristics and yielded wind pressure coefficients on the building′s front face that closely matched WT experiment. Thus, the power spectral densities in the along-wind force showed good agreement.

The slight difference in regions of negative pressures highlights the need for further improvement. Continued development will enhance the accuracy of LES in capturing complex wind effects on structures.

Acknowledgement: The authors gratefully acknowledge Professor Hiroshi Noda of Kindai University for his valuable guidance and advice throughout this research. The authors also wish to thank the Information Technology Center at the University of Tokyo for providing access to the High-Performance Computing system through the corporate use program.

References

1) 日本建築学会: 建築物荷重指針・同解説 , 2015
2) 日本建築学会: 建築物の風応答・風荷重評価/CFD 適用ガイド, 2017
3) Doan S. L., Kojima C., Kawashima M., and Noda H.: Estimating grid spacing in laboratory-scale Large Eddy Simulations: Insights from the Kolmogorov energy spectrum, 風工学シンポジウム論文集 第 28 巻, 2024
4) Aboshosha H., Ahmed E., Girma T. B., and Ashraf E. D.: Consistent inflow turbulence generator for LES evaluation of wind-induced responses for tall buildings, Journal of Wind Engineering and Industrial Aerodynamics, Vol.142, pp.198-216, 2015
5) Hoshiya M.: Simulation of multi-correlated random processes and application to structural vibration problems, 土木学会論文集, 土木学会, 1972
6) Kondo K., Murakami S., and Mochida A.: Generation of velocity fluctuations for inflow boundary condition of LES, Journal of Wind Engineering and Industrial Aerodynamics, Vol.67-68, pp.51-64, 1997
7) Noda H. and Nakayama A.: Reproducibility of flow past two-dimensional rectangular cylinders in a homogeneous turbulent flow by LES, Journal of wind engineering and industrial aerodynamics, Vol.91(1-2), pp.265-278, 2003
8) Noda H., Nakayama A., Miyashita K., and Taishida T.: Turbulent boundary layer generated using stochastic method for inflow conditions of LES, International Journal of Advances in Engineering Sciences and Applied Mathematics, Vol.10, pp.146-158, 2018
9) Kraichnan R. H.: On Kolmogorov's inertial-range theories, Journal of Fluid Mechanics, Vol.62(2), pp.305-330, 1974
10) Smirnov A., Shi S., and Celik I.: Random flow generation technique for large eddy simulations and particle-dynamics modeling, J. Fluids Eng., Vol.123(2), pp.359-371, 2001
11) Huang S. H., Li Q.S., and Wu J.R.: A general inflow turbulence generator for large eddy simulation, Journal of Wind Engineering and Industrial Aerodynamics, Vol.98(10), pp.600-617, 2010
12) Tokyo Polytechnic University: The 21st Century COE program: Wind Effects on Buildings and Urban Environment, https://www.wind.arch.t-kougei.ac.jp/info_center/windpressure/highrise/Homepage/homepageHDF.htm (Accessed 7 July 2025)
13) Counihan J.: Adiabatic atmospheric boundary layers: a review and analysis of data from the period 1880–1972, Atmospheric Environment (1967), Vol.9(10), pp.871-905, 1975
14) Yu Y., Yi Y., and Zhuangning X.: A new inflow turbulence generator for large eddy simulation evaluation of wind effects on a standard high-rise building, Building and Environment, Vol.138, pp.300-313, 2018
15) Chen L., Chao L., Jinghan W., Gang H., Qingxing Z., Qingfeng Z., and Yiqing X.: Consistency improved random flow generation method for large eddy simulation of atmospheric boundary layer, Journal of Wind Engineering and Industrial Aerodynamics, Vol.229, pp.105-147, 2022